# Characterization of PbO-B$_2$O$_3$-GeO$_2$-La$_2$O$_3$ and PbO-B$_2$O$_3$-SiO$_2$-ZnO glasses: refractive, acoustic, photo-elastic and acousto-optic properties

[1] Krupych O., [1] Martynyuk-Lototska I., [1] Say A., [1] Boyko V., [2] Goleus V., [2] Hordieiev Y. and [1] Vlokh R.

[1] O.G. Vlokh Institute of Physical Optics, 23 Dragomanov Street, 79005 Lviv, Ukraine, ok@ifo.lviv.ua
[2] Ukrainian State University of Chemical Technology, 8 Gagarin Street, 49005 Dnipro, Ukraine

**Abstract**. New high-lead glasses with two different compositions are subjected to comprehensive material characterization. In particular, their refractive indices, optical transmission spectra, photo-elastic, piezo-optic and strain-optic constants, ultrasound velocities and elastic constants are measured. We find the short-wavelength absorption edges as $\lambda_{edge} = 383$ and 475 nm for these compounds. The acousto-optic figures of merit are calculated for the glasses under study. Their maximal acousto-optic figures of merit turn out to be higher than the corresponding values for fused silica and dense flint glasses, which are known as vitreous materials widely used in serial acousto-optic modulators.

## 1. Introduction

Acousto-optic (AO) methods for controlling optical radiation are widely used in various AO devices, such as modulators, deflectors and frequency shifters [1]. AO diffraction consists in interaction of optical waves with the phase gratings caused by acoustic waves through an elasto-optic effect. The efficiency of these devices is primarily defined by the AO medium, which has to be characterized by high enough AO figure of merit $M_2$ [2]. Moreover, any good AO material must reveal low acoustic losses in the operating frequency range, optical transparency in the working spectral range, high chemical resistance and satisfactory mechanical strength [3]. Simple and cheap technology of synthesis is also desirable.

Nowadays, the AO properties of a large number of materials, both single crystals and glasses, have been investigated. Nevertheless, the problem of searching for new high-performance AO materials is still urgent. Vitreous materials, unlike single crystals, are of greater interest here because of simple technology of their synthesis, a great variety of shapes and sizes, high optical isotropy and homogeneity, low cost and so on. The glasses are widely used in modern optics, laser technology and optoelectronics [4].

Among AO glasses (see Table 1), the glasses with high refractive index and AO figure of merit $M_2$ and good optical transparency in the working spectral interval are the most commonly used [5, 6]. The above set of properties can often be achieved in the glasses with high contents of lead oxide [3, 4, 7], which can be as high as 90 mol. %. This has led us to study the glasses of PbO-B$_2$O$_3$-GeO$_2$-La$_2$O$_3$ and PbO-B$_2$O$_3$-SiO$_2$-ZnO system [8, 9]. The aims of this work are to characterize these two high-lead glasses optically and estimate their prospects as AO materials.

**Table 1**. Refractive indices, optical transmission regions and AO figures of merit known for some AO glasses.

| Glass | Transmission range, μm | Refractive index (at $\lambda = 632.8$ nm) | AO figure of merit, $10^{-15}$ s$^3$/kg |
|---|---|---|---|
| Fused silica (SiO$_2$) [5, 10] | 0.20–4.0 | 1.457 | 1.56 |
| Schott dense flint SF 4 [5] | 0.38–1.8 | 1.749 | 3.0 |
| LZOS dense flint TF-8 [11] | 0.39–2.5 | 1.685 | 4.2 |
| LZOS dense flint TF-7 [11, 12] | 0.40–2.6 | 1.723 | 5.12 |
| Schott dense flint SF 8 [6] | 0.39–2.4 | 1.686 | 6.3 |
| Schott dense flint SF 6 [10] | 0.45–2.0 | 1.799 | 8.0 |
| Schott dense flint SF 59 [5] | 0.46–2.5 | 1.943 | 12.6 |
| Tellurite Hoya AOT 44B [5] | 0.43–2.5 | 1.971 | 20.9 |
| Tellurite Hoya AOT 5 [5] | 0.47–2.7 | 2.090 | 23.9 |
| Chalcogenide Ge$_{55}$As$_{12}$S$_{33}$ [5] | 1.00–14.0 | – | 54 |
| Arsenic trisulfide (As$_2$S$_3$) [5] | 0.60–11.0 | 2.465 | 256 |

## 2. Experimental methods

In this work we characterize high-lead glasses of the two following compositions. The glass compound 1 consists of 50 mol. % PbO, 25% B$_2$O$_3$, 20% GeO$_2$ and 5% La$_2$O$_3$, while the compound 2 includes 55 mol. % PbO, 30% B$_2$O$_3$, 10% SiO$_2$ and 5% ZnO. The batches prepared in this way have been melted in a platinum crucible (50 ml), which is placed inside electric furnace with silicon-carbide heaters. This process has been performed at 950–1050°C and lasted for 60 min. The initial materials include lead tetroxide, boric acid, quartz grits, germanium dioxide, zinc oxide and lanthanum oxide. Glass samples for our studies have been made by casting glass melt in steel molds, followed by annealing in a muffle furnace at 300°C. The dilatometric softening temperatures have been $T_{d1} = 345$°C for the compound 1 and $T_{d2} = 330$°C for the compound 2. Their coefficients of linear thermal expansion are equal to $\alpha_1 = 95.0 \times 10^{-6}$ K$^{-1}$ and $\alpha_2 = 10.7 \times 10^{-6}$ K$^{-1}$, and the densities are $\rho_1 = 6250$ kg/m$^3$ and $\rho_2 = 6306$ kg/m$^3$, respectively. The glass samples have a disk-like shape, with the diameters approximately equal to 25 mm and the thicknesses $t_1 = 2.91$ mm and $t_2 = 4.03$ mm respectively for the compounds 1 and 2.

The transmission spectra of the both glass samples have been studied using a Lambda 25 spectrophotometer at the light wavelength from 200 nm to 1100 nm, i.e. in the visible, near ultraviolet and near infrared ranges.

The refractive indices of the glasses have been measured with ellipsometric and prism methods. A standard technique based on PCSA ellipsometer LEF-3M has been used, with seven different incident angles for error minimization. It is known that the accuracy of ellipsometric measurements depends notably on the quality of sample surfaces. Since raw (non-processed) samples have been used in our experiments, this technique is express one, though it does not ensure high precision.

Another technique applied to measure the refractive indices is a refractometric method, which is based on a Littrow prism arranged under condition of autocollimation [13–16]. The simplicity of optics inherent to this technique and the measurement accuracy achieved are comparable to those of a commonly known minimum-deviation method. However, our system (see Fig. 1a) differs substantially from the standard minimum-deviation setup. It tracks the signal beam by rotating prism only, while the other elements of optical scheme remain fixed. This reduces the
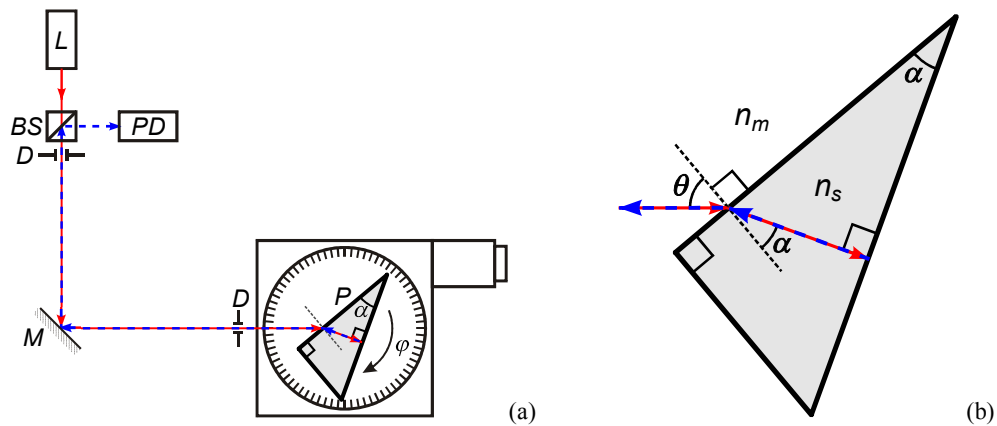
**Fig. 1.** (a) Experimental setup for monitoring the angular position of a prism with the probing light reflected normally to the rear face of the prism: *L* – laser, *BS* – beam splitter, *D* – pinhole diaphragm, *M* – mirror, *PD* – photodetector, *P* – prism with apex angle *α*, and *φ* – azimuth of the prism mounted on rotation stage. (b) Reflection of probing light normal to the rear face of Littrow prism.

corresponding errors. The use of the probing laser beam incident at the prism makes the system extremely easy to assemble and exploit. As a result, our system presents a simple and convenient means for measuring the refractive index with high accuracy.

The principle of measurements based upon the Littrow prism under condition of autocollimation is illustrated in Fig. 1b. If the refraction angle of the probing light at the front face of the prism equals to the apex angle *α*, then the light propagates along the normal to the rear face of the prism. The refractive index $n_S$ of the sample prism can be determined from the Snell's law:

$$n_S = n_m \frac{\sin\theta}{\sin\alpha}, \tag{1}$$

where $n_m$ is the refractive index of the ambient medium ($n_m = 1.00027$ in the case of air) and $\theta$ the incident angle. The incident light is split into transmitted and reflected light at the interface between the materials with different refractive indices. When the probing light is normally aligned to the rear face of the prism, a part of this light is reflected along the same path but in the opposite direction (see Fig. 1b).

The prism is placed on a motorized rotation stage with the minimal angular step 0.01°. The reflected light retraces its path so that it passes through the both diaphragms, reflects at the beam splitter and is finally detected by a photodiode. With full revolution of the rotation stage, four azimuthal positions of the prism ($\varphi_0$, $\varphi_1$, $\varphi_2$ and $\varphi_3$) are detected, each of which satisfying the autocollimation condition (see Fig. 2).
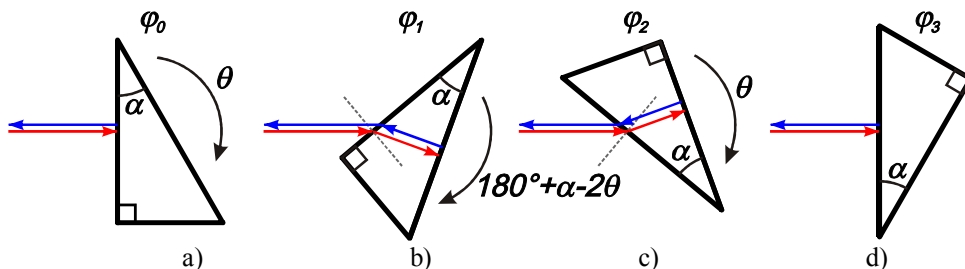


**Fig. 2.** Orientations of right-angled triangular prism under condition of autocollimation, as achieved during prism rotation: (a) reflection from the front leg corresponds to azimuthal position $\varphi_0$, (b) reflection from the rear hypotenuse to $\varphi_1$, (c) reflection from the rear leg to $\varphi_2$, and (d) reflection from the front hypotenuse to $\varphi_3$.

Azimuthal dependences of the intensity detected by a photodiode-based photodetector in the vicinities of the autocollimation condition for the test prism are presented in Fig. 4. These dependences are fitted by the Gaussian function and the positions of maxima are calculated with the errors not exceeding 0.0004°. In such a manner, azimuthal positions $\varphi_0$, $\varphi_1$, $\varphi_2$ and $\varphi_3$ can be determined. Then the incident angle $\theta$ and the apex angle $\alpha$ are calculated:

$$\delta_1 = \varphi_1 - \varphi_0, \quad \delta_2 = \varphi_2 - \varphi_0, \quad \delta_3 = \varphi_3 - \varphi_0, \quad \theta = \frac{1}{2}(\delta_1 + \delta_3 - \delta_2), \quad (2)$$

$$\alpha = \frac{1}{2}(\delta_1 + \delta_2 + \delta_3 - 360°). \quad (3)$$

After that the refractive index of the prism can be calculated with Eq. (1). It is worth stressing that, in frame of this method, the apex angle of the prism is determined in the course of measurements. This makes sample preparation simpler because there is no need to provide some predefined apex angle with high precision.

To check the accuracy of our method and experimental setup, we have determined the refractive index of the test prism with the nominal apex angle 30° at the wavelength of He-Ne laser ($\lambda = 632.8$ nm). This test sample is made of BK7 glass. The following azimuthal positions, which satisfy the autocollimation condition, have been determined: $\varphi_0 = 43.9036°\pm0.0003°$, $\varphi_1 = 93.1343°\pm0.0004°$, $\varphi_2 = 204.6762°\pm0.0002°$ and $\varphi_3 = 253.8881°\pm0.0003°$ (see Fig. 4). Then the incident angle $\theta$ and the apex angle $\alpha$ have been calculated as $\theta = 49.2213°\pm0.0006°$ and $\alpha = 29.9939°\pm0.0008°$. As a result, the refractive index has been determined as $n_S = 1.51516\pm0.00004$. This value is only slightly larger than the index known for the Schott N-BK7 glass at the same wavelength (1.51509). This confirms high enough precision of our method and setup. If good flatness of the prism faces and a sufficient homogeneity of the material are provided, the refractive index can be measured with at least fourth decimal digit reliable.
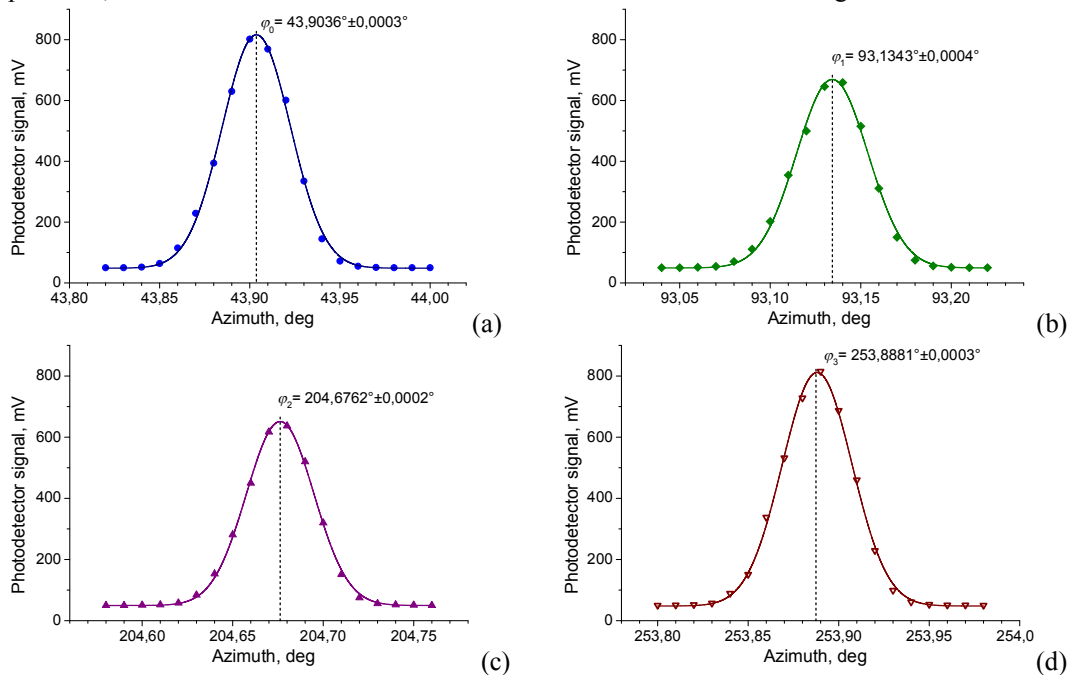


**Fig. 4.** Intensity detected by photodiode as a function of angular position for the test 30°-prism of BK7 glass in the vicinity of azimuths $\varphi_0$ (a), $\varphi_1$ (b), $\varphi_2$ (c) and $\varphi_3$ (d). Experimental data are depicted by symbols and Gaussian fittings as solid lines.

The acoustic-wave velocities have been measured with a pulse-echo overlap technique [17]. The acoustic waves in the samples are excited by means of LiNbO₃ transducers (the resonance frequency $f = 10$ MHz, the bandwidth $\Delta f = 0.1$ MHz, and the acoustic power $P_a = 1–2$ W). For the acoustic wave-velocity studies, we have prepared the samples which have the dimensions $2.90 \times 6 \times 20$ mm³ for the compound 1 and $4.025 \times 6 \times 20$ mm³ for the compound 2.

Following from the density $\rho$ and the velocities $v_\parallel$ and $v_\perp$ of the longitudinal and shear acoustic waves, one can calculate the elastic constants of the glasses under test. These are the shear modulus $G$, the Young's modulus $E$, the Poisson's ratio $v$ and the effective compliance constant $S_{ef}$. The appropriate relations are as follows [18]:

$$G = \rho v_\perp^2, \tag{4}$$

$$v = \frac{v_\parallel^2 - 2v_\perp^2}{2\left(v_\parallel^2 - v_\perp^2\right)}, \tag{5}$$

$$E = 2G(1+v), \tag{6}$$

$$S_{ef} = -v/E. \tag{7}$$

We have used an original experimental technique for measuring piezo-optic coefficients. It is based on a 2D digital interferometry and four-point bending applied to a bar-shaped sample [19–21]. Two glass samples have been prepared for these experiments. Their dimensions amount to $2.9 \times 5.2 \times 18.1$ mm³ and $4.03 \times 5.0 \times 18.2$ mm³ respectively for the cases of compounds 1 and 2. The measuring procedures include the next steps. First, the input polarization of a He-Ne laser (the wavelength $\lambda = 632.8$ nm) is set in a vertical plane and an interferogram for the free sample is recorded. Then a loading force is applied to the sample and a relevant interferogram is recorded again. After that, the same procedures are repeated for the horizontal input polarization.

## 3. Results and discussion

The optical transmission spectra are presented in Fig. 5. The short-wavelength absorption edges are detected as $\lambda_{edge} = 383$ nm for the compound 1 and $\lambda_{edge} = 475$ nm for the compound 2. The refractive indices obtained using the ellipsometric method are equal to $n_{1E} = 1.9342 \pm 0.0007$ and $n_{2E} = 1.9456 \pm 0.0022$ for the compounds 1 and 2, respectively.
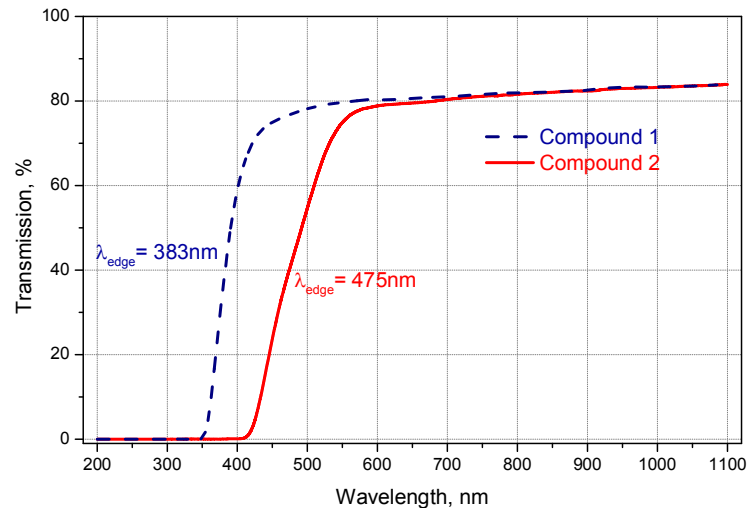


**Fig. 5.** Optical transmission spectra measured for the glass compounds 1 and 2.

To determine the refractive indices of our glasses by the prism-autocollimation technique, two prisms were prepared for every composition (i.e., four prisms in total) with the apex angles close to 24°. Each prism has been explored twice: when lying on one side (△) and on the opposite side (▽). This means that the refractive index for each glass compound has been calculated as an average of the four independent measurements. The refractive indices $n_{1P}(632.8) = 1.9360 \pm 0.0023$ and $n_{2P}(632.8) = 1.9749 \pm 0.0017$ are obtained for the compounds 1 and 2 at the wavelength $\lambda = 632.8$ nm. These refractive indices are somewhat higher than those obtained with the ellipsometric method. This can be explained by a conceptual difference between the reflection of light by any material and its transmission inside this material and, besides, by the influence of surface quality. The errors are higher than those typical for the test prism, because of lower perfection of our samples (a moderate flatness of the prism faces due to their small thickness) and less inhomogeneity of our glass materials. For the compound 1 we have obtained a higher error of the prism method, if compared with the ellipsometric method. As demonstrated below, this glass composition has a more significant inhomogeneity. This circumstance deteriorates essentially the measurement accuracy due to a volume character of our experiments, in contrast with the ellipsometry experiments in which the light interacts locally with a thin surface layer of sample.

Using the prism-autocollimation method, we have also determined the refractive indices of the both glass compounds at the green-laser wavelength $\lambda = 532$ nm. The values $n_{1P}(532) = 1.9550 \pm 0.0023$ and $n_{2P}(532) = 2.0063 \pm 0.0018$ have been obtained respectively for the compounds 1 and 2.

The velocities of the acoustic waves and the elastic constants (the shear modulus $G$, the Young's modulus $E$, the Poisson's ratio $v$ and the effective compliance constant $S_{ef}$) derived experimentally for our glasses are presented in Table 2.

**Table 2.** Acoustic-wave velocities and elastic parameters of our glasses.

| Parameter | Compound 1 | Compound 2 |
|---|---|---|
| Longitudinal wave velocity $v_{11} = v_{\parallel}$, m/s | 3393±6 | 3164±9 |
| Shear wave velocity $v_{12} = v_{\perp}$, m/s | 1896±5 | 1747±8 |
| Mass density $\rho$, kg/m$^3$ | 6250±26 | 6306±34 |
| Shear modulus $G$, GPa | 22.47±0.13 | 19.25±0.16 |
| Poisson's ratio $v$ | 0.2730±0.0021 | 0.2807±0.0034 |
| Young's modulus $E$, GPa | 57.20±.033 | 49.30±0.44 |
| Effective compliance $S_{ef} = -v/E$, Brewster | −4.772±0.046 | −5.694±0.085 |

Typical interferograms of the central parts of samples of the glass compounds 1 and 2 are shown respectively in Fig. 6 and Fig. 7. As seen from Fig. 6, the interference fringes are highly distorted, thus proving a significant inhomogeneity of the glass compound 1 (see also above).

After recording the interferograms, we have processed them with specially developed original software described in our earlier work [20]. This has yielded in the combined photo-elastic coefficient $Q$, which accounts both the piezo-optic change in the refractive indices and the Poisson's strain-related change in the optical path length. This combined photo-elastic coefficient $Q$ can be expressed [19] as $Q_i = K_i + D$, where $K_i = -n^3 \pi_{1i}/2$ is the photo-elastic constant and $D = S_{ef}(n-1)$ is the strain term. When the combined photo-elastic coefficient $Q_i$, the refractive index $n$ and the effective compliance $S_{ef}$ are known, the photo-elastic constants $K_{\parallel}$ and $K_{\perp}$ can be calculated:

$$K_i = Q_i - S_{ef}(n-1). \tag{8}$$
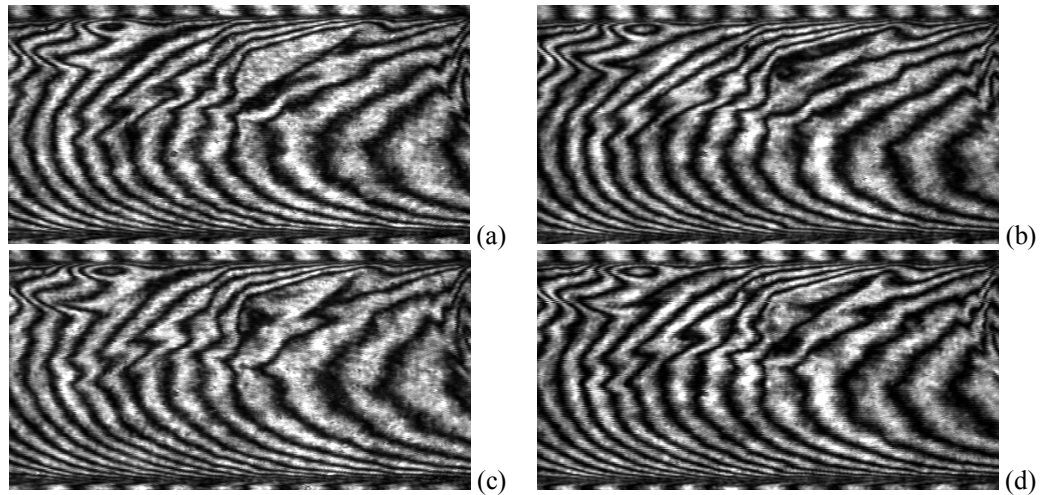
**Fig. 6.** Interferograms obtained for the sample of glass compound 1: (a) free sample (vertical polarization), (b) free sample (horizontal polarization), (c) loaded sample (vertical polarization), and (d) loaded sample (horizontal polarization). Loading force is equal to 48.9 N and wavelength to $\lambda$ = 632.8 nm.
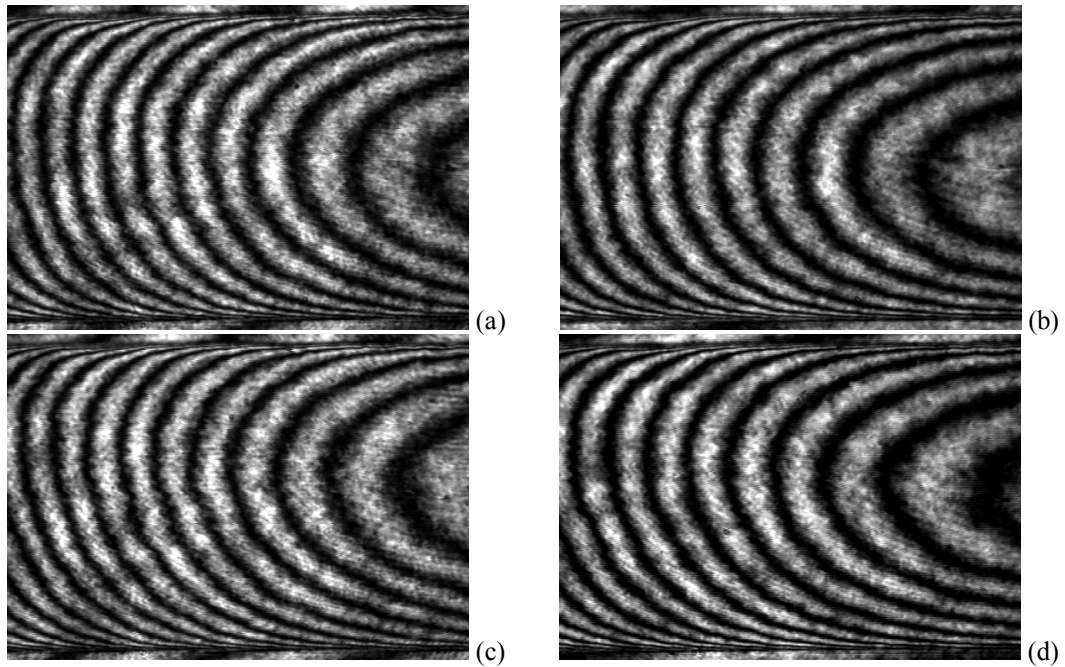


**Fig. 7.** Interferograms obtained for the sample of glass compound 2: (a) free sample (vertical polarization), (b) free sample (horizontal polarization), (c) loaded sample (vertical polarization), and (d) loaded sample (horizontal polarization). Loading force is equal to 57.1 N and wavelength to $\lambda$ = 632.8 nm.

Then the stress-optic coefficient $K$, which represents a standard parameter of glasses, is calculated as $K = K_\parallel - K_\perp$. After that the piezo-optic coefficients $\pi_{1i}$ are calculated, using the experimental photo-elastic constants $K_\parallel$ and $K_\perp$:

$$\pi_{11} = \pi_\parallel = -\frac{2K_\parallel}{n^3}; \quad \pi_{12} = \pi_\perp = -\frac{2K_\perp}{n^3}. \tag{9}$$

Finally, the strain-optic coefficients $p_{11}$ and $p_{12}$ are calculated issuing from the piezo-optic coefficients and the elastic modules $E$ and $v$ [19]:

$$p_{11} = \frac{E\left[(1-\nu)\pi_{11} + 2\nu\pi_{12}\right]}{(1+\nu)(1-2\nu)}; \qquad p_{12} = \frac{E(\pi_{12} + \nu\pi_{11})}{(1+\nu)(1-2\nu)}. \tag{10}$$

All of these photo-elastic parameters for our glass compounds are collected in Table 3.

**Table 3.** Experimental values of photo-elastic parameters of our glasses at the wavelength $\lambda = 632.8$ nm (in Brewsters).

| Parameter | | Compound 1 | Compound 2 |
|---|---|---|---|
| Combined photo-elastic coefficients | $Q_\parallel$ | −9.304±0.204 | −12.314±0.241 |
| | $Q_\perp$ | −11.783±0.251 | −11.002±0.215 |
| Strain-related term | $D = S_{ef}(n-1)$ | −4.462±0.043 | −5.552±0.083 |
| Photo-elastic constants | $K_\parallel$ | −4,842±0,208 | −6.761±0.255 |
| | $K_\perp$ | −7.320±0.255 | −5.450±0.231 |
| Stress-optic coefficient | $K = K_\parallel - K_\perp$ | 2.478±0.329 | −1.311±0.344 |
| Piezo-optic coefficients | $\pi_{11} = \pi_\parallel$ | 1.337±0.058 | 1.755±0.066 |
| | $\pi_{12} = \pi_\perp$ | 2.021±0.070 | 1.415±0.060 |
| | $\pi_{44} = \pi_{11} - \pi_{12}$ | −0.684±0.091 | 0.340±0.089 |
| Elasto-optic coefficients | $p_{11}$ | 0.205±0.006 | 0.181±0.006 |
| | $p_{12}$ | 0.236±0.008 | 0.167±0.006 |
| | $p_{44} = (p_{11} - p_{12})/2$ | −0.015±0.005 | 0.007±0.004 |

The main parameter that characterizes the AO efficiency of any optical material is its AO figure of merit $M_2$ [2]. It is expressed as

$$M_2 = \left(n^6 p_{ef}^2\right)\Big/\left(\rho v_{ef}^3\right), \tag{11}$$

where $n$ denotes the refractive index, $p_{ef}$ the effective elasto-optic coefficient, $v_{ef}$ the velocity of the effective acoustic wave, and $\rho$ the material density.

It is known [22] that isotropic solids like glasses can manifest three different types of AO interactions, two types for the longitudinal acoustic waves and one type for the shear wave. The AO figure of merit for the interaction type (I) is expressed as

$$M_2^{(I)} = \left(n^6 p_{12}^2\right)\Big/\left(\rho v_{11}^3\right). \tag{12}$$

We remind that, for the type (I), the polarization of the incident and diffracted optical waves is normal to the propagation direction of the longitudinal acoustic wave with the velocity $v_{11}$, i.e. normal to the interaction plane. For the interaction type (II), the polarization of the incident and diffracted optical waves is almost parallel to the propagation direction of the longitudinal acoustic wave with the velocity $v_{11}$, i.e. it lies in the interaction plane. Then we have

$$M_2^{(II)} = \left(n^6 p_{11}^2\right)\Big/\left(\rho v_{11}^3\right). \tag{13}$$

Finally, in case of the interaction type (III) the polarization of the incident and diffracted optical waves, as well as the polarization of the shear acoustic wave with the velocity $v_{12}$, lie inside the interaction plane. Then we obtain

$$M_2^{(III)} = \left(n^6 p_{44}^2\right)\Big/\left(\rho v_{12}^3\right). \tag{14}$$

Having known the refractive indices, the strain-optic coefficients, the densities and the

acoustic velocities, we are now able to calculate the AO figures of merit for our glasses. The relevant results are collected in Table 4. As seen from Table 4, the AO figure of merit for the interaction type (III) is much less than those found for the types (I) and (II), in spite of the fact that the velocities of the shear acoustic waves are about a half of the velocities typical for the longitudinal waves (see Eq. (11)). The reason is that the effective elasto-optic coefficient $p_{44}$ for the interaction type (III) is much less than the coefficients $p_{11}$ and $p_{12}$ responsible for the types (I) and (II).

**Table 4.** AO figures of merit of our glasses (in $10^{-15}$ s$^3$/kg), as calculated for the AO interaction types (I), (II) and (III) at the wavelength $\lambda = 632.8$ nm.

| Glass | $M_2^{(I)}$ | $M_2^{(II)}$ | $M_2^{(III)}$ |
|---|---|---|---|
| Compound 1 | 13.55±0.61 | 10.25±0.44 | 0.33±0.15 |
| Compound 2 | 8.33±0.45 | 9.68±0.46 | 0.08±0.07 |

Finally, we note that the maximal AO figures of merit for our glasses are almost 8.7 times (for the compound 1) or 6.2 times (for the compound 2) higher than the maximal AO figure of merit known for fused silica ($M_2 = 1.56 \times 10^{-15}$ s$^3$/kg), which represents a widely used AO material. Moreover, they are also higher than the AO figure of merit typical for the dense flint glasses TF-7 ($M_2 = 5.1 \times 10^{-15}$ s$^3$/kg) and SF 6 ($M_2 = 8 \times 10^{-15}$ s$^3$/kg), which are commonly used in serial AO modulators.

## 4. Conclusion

The new lead-based glasses of the two different compositions are characterized optically. The glass compound 1 includes 50 mol. % PbO, 25% B$_2$O$_3$, 20% GeO$_2$ and 5% La$_2$O$_3$, while the compound 2 consists of 55 mol. % PbO, 30% B$_2$O$_3$, 10% SiO$_2$ and 5% ZnO. We have measured the optical transmission spectra in the near-UV, visible and near-IR spectral ranges. Short-wavelength absorption edges are detected at $\lambda_{edge} = 383$ nm and $\lambda_{edge} = 475$ nm for the compounds 1 and 2, respectively. The refractive indices of the both glasses are determined by means of the ellipsometric and prism-autocollimation techniques. The ultrasound velocities are measured and the elastic constants are derived for the both compounds. The piezo-optic and elasto-optic coefficients are determined using the 2D laser digital interferometric technique and the four-point bending. The elasto-optic coefficients and the AO figures of merit are calculated. The maximal AO figures of merit obtained for our glasses are higher than those typical for fused silica and dense flint glasses, which are widely used in serial AO modulators.

## References

1. Chang I C. Acousto-optic devices and applications. Ch.12, Acousto-optic devices and applications. In: Handbook of optics (Vol. II). Ed by M Bass. McGraw-Hill (1995).
2. Smith T and Korpel A, 1965. Measurement of light-sound interaction efficiencies in solids. IEEE J. Quant. Electron. **1**: 283–284.
3. Rabukhin A I, 1995. Acoustooptical efficiency of germanate glasses containing lead and bismuth oxides. Glass and Ceramics. **52**: 203–206.
4. Abdel-Baki M and El-Diasty F, 2013. Glasses for photonic technologies. Int. J. Opt. Appl. **3**: 125–137.
5. Weber M J. Handbook of optical materials. Boca Raton, Filadelphia: CRC Press (2003).
6. Eschler H and Weidinger F, 1975. Acousto-optic properties of dense flint glasses. J. Appl. Phys. **46**: 65–70.

7.  Parshikov S A, Zaytsev A I, Zamkov A V and Shabanova L A, 1998. Acousto-optic properties of oxide glasses with high polarized ions. Fizika i Chimiya Stekla. **24**: 829–832.

8.  Goleus V I, Hordieiev Y S and Nosenko A V, 2018. Properties of low-melting glasses in the system PbO–ZnO–B$_2$O$_3$–SiO$_2$. Voprosy Khimii i Khimicheskoi Tekhnologii. **4**: 92–96.

9.  Goleus V I and Hordieiev Y S 2018. Calculation of optical constants of glasses in the PbO–B$_2$O$_3$–SiO$_2$–GeO$_2$ oxide system. Voprosy Khimii i Khimicheskoi Tekhnologii, **5**: 92–96.

10. http://www.brimrose.com/pdfandwordfiles/aointro.pdf

11. Semenov V and Sheloput D, 1979. Acousto-optic characteristics of dense and super dense flints. Avtometriya. **2**: 93–95.

12. Kludzin V V, Kulakov S V, Razzhivin B P and Ulyanov V K, 1972. The possibility of application of dense flints for ultrasonic light modulation. Optiko-Mechanicheskaya Promyshlennost. **1:** 3–5.

13. Cheng C C, 2014. Refractive index measurement by prism autocollimation. Amer. J. Phys. **82**: 214–216.

14. Werner A J, 1968. Methods in high precision refractometry of optical glasses. Appl. Opt. **7**: 837–843.

15. Astrua M and Pisani M, 2009. Prism refractive index measurement at INRiM. Meas. Sci. Technol. **20**: 095305-1–7.

16. Ilev I K, 1995. Simple autocollimation laser refractormeter with highly sensitive, fiber-optic output. Appl. Opt. **34**: 1741–1743.

17. Papadakis E P, 1967. Ultrasonic pulse velocity by the pulse-echo overlap method incorporating diffraction phase correlation. J. Acoust. Soc. Amer. **42**: 1045–1051.

18. Kino G S. Acoustic waves: devices, imaging, and analog signal processing (Vol. 107). Englewood Cliffs, N J: Prentice-Hall (1987).

19. Krupych O, Savaryn V, Skab I and Vlokh R, 2011. Interferometric measurements of piezooptic coefficients by means of four-point bending method. Ukr. J. Phys. Opt. **12**: 150–160.

20. Krupych O, Savaryn V, Krupych A, Klymiv I and Vlokh R, 2013. Determination of piezo-optic coefficients of crystals by means of four-point bending. Appl. Opt. **52**: 4054–4061.

21. Vlokh R O, Skab I P, Krupych O M and Adamenko D I. Methods of piezo-optics in inhomogeneous mechanical fields. Lviv: Publishing House of Vlokh Institute of Physical Optics (2019).

22. Mys O, Kostyrko M, Smyk M, Krupych O and Vlokh R, 2014. Anisotropy of acousto-optic figure of merit in optically isotropic media. Appl. Opt. **53**: 4616–4627.

*Анотація. Охарактеризовано нові сорти скла з високим вмістом свинцю двох різних складів. Зокрема, визначено їхні показники заломлення, спектри оптичного пропускання, фотопружні, п'єзооптичні та пружнооптичні постійні, швидкості ультразвуку та пружні константи. Для цих сполук визначено короткохвильові краї поглинання λ$_{edge}$ = 383 і 475 нм. Розраховано коефіцієнти акустооптичної якості для досліджуваних сортів скла. Їхні максимальні акустооптичні показники виявилися вищими за відповідні значення для плавленого кварцу та важких флінтів. Останні відомі як склоподібні матеріали, що широко використовуються в серійних акустооптичних модуляторах.*